

HUBBLE SPACE TELESCOPE NEAR-INFRARED AND OPTICAL IMAGING OF FAINT RADIO SOURCES IN THE DISTANT CLUSTER CL 0939+4713

IAN SMAIL,¹ G. MORRISON,² M. E. GRAY,³ F. N. OWEN,² R. J. IVISON,⁴ J.-P. KNEIB⁵ & R. S. ELLIS³

1) Department of Physics, University of Durham, South Road, Durham DH1 3LE, UK

2) NRAO, P.O. Box 0, 1003 Lopezville Road, Socorro, NM 87801

3) Institute of Astronomy, Madingley Road, Cambridge CB3 OHA, UK

4) Department of Physics and Astronomy, University College London, Gower Street, London WC1E 6BT, UK

5) Observatoire Midi-Pyrénées, CNRS-UMR5572, 14 Avenue E. Belin, 31400 Toulouse, France

Received 1999 March 5; accepted: 1999 --

ABSTRACT

We present deep *Hubble Space Telescope NICMOS* near-infrared and *WFPC2* optical imaging of a small region in the core of the distant rich cluster Cl 0939+4713 ($z = 0.41$). We compare the optical and near-infrared morphologies of cluster members and find apparent small-scale optical structures within the galaxies which are absent in the near-infrared. We conclude that strong dust obscuration is a common feature in the late-type galaxies in distant clusters. We then concentrate on a sample of ten faint radio galaxies lying within our *NICMOS* field and selected from a very deep 1.4-GHz VLA map of the cluster with a 1σ flux limit of $9\mu\text{Jy}$. Using published data we focus on the spectral properties of the eight radio-selected cluster members and show that these comprise a large fraction of the post-starburst population in the cluster. The simplest interpretation of the radio emission from these galaxies is that they are currently forming massive stars, contradicting their classification as post-starburst systems based on the optical spectra. We suggest that this star formation is hidden from view in the optical by the same obscuring dust which is apparent in our comparison on the optical and near-infrared morphologies of these galaxies. We caution that even in the restframe optical the effects of dust cannot be ignored when comparing samples of distant galaxies to low-redshift systems, particularly if dust is as prevalent in distant galaxies as appears to be the case in our study.

Subject headings: galaxies: evolution — galaxies: clusters: individual Cl 0939+4713 (A 851) — galaxies: starburst — radio continuum: galaxies — infrared: galaxies

1. INTRODUCTION

The characteristics of the galaxy populations in the cores of rich clusters appear to vary strongly as a function of redshift, with an increasing fraction of blue galaxies in clusters at $z > 0.2$ (the Butcher-Oemler effect, Butcher & Oemler 1984). The search for the processes responsible for these rapid changes has become a vigorous field of research and at least for the blue cluster galaxies a broad consensus has been reached about the nature of this population. The bulk are star-forming cluster members, they cover a wide range of luminosities, from a few L^* downwards, and have emission line strengths which indicate moderate to high star formation rates (Abraham et al. 1996; Balogh et al. 1999; Barger et al. 1996; Couch & Sharples 1987; Dressler & Gunn 1992; Dressler et al. 1999, D99; Fabricant et al. 1994; Fisher et al. 1998; Lavery & Henry 1988). The optical morphologies of these galaxies were investigated firstly with high-resolution ground-based (Lavery et al. 1992) and more recently with *Hubble Space Telescope (HST)* imaging (Dressler et al. 1994a; Couch et al. 1994, 1998; Oemler et al. 1997; Smail et al. 1997, S97; Fabricant et al. 1999). These studies have shown that most of the blue star-forming galaxies have strong disk components and a large fraction also appear to be disturbed, with structures suggesting mergers or tidal interactions. Thus the increasing proportion of blue galaxies within distant clusters is associated with an increasing number of

actively star-forming disk galaxies in these environments. The large fraction of apparently disturbed galaxies suggests that galaxy-galaxy interactions or the effects of the cluster tidal field on these disk galaxies could be responsible for the Butcher-Oemler effect (Moore, Lake & Katz 1998).

The spectroscopic studies of distant clusters uncovered another population of luminous galaxies which is not seen in similar numbers in local clusters. These are galaxies with strong Balmer absorption (typically measured using the H δ $\lambda 4104\text{\AA}$ line and coming predominantly from A stars) and no [OII] $\lambda 3727\text{\AA}$ emission. The large population of A stars is a sign that the galaxy was actively forming massive stars in the recent past ($\lesssim 1\text{Gyr}$), while the lack of emission lines suggests that this star formation has now ceased. Together the spectral properties are interpreted as showing that the galaxy is in a post-starburst phase. Almost 20% of the luminous galaxies within the cores of distant clusters fall in this post-starburst class (e.g. D99, although see Balogh et al. 1999) and it has been suggested that this high fraction indicates that almost all cluster galaxies pass through this phase (Barger et al. 1996).

There is an increasing realisation in the community of the importance of dust obscuration in defining the apparent properties of galaxies in the near-UV and optical, particularly at high redshifts. This issue has been highlighted by the disagreement over the form of the star formation history of the Universe as estimated from the variation in

the ultraviolet luminosity density with redshift (e.g. Lilly et al. 1996; Steidel et al. 1999) compared to star formation indicators at longer wavelengths such as H α emission (Yan et al. 1999) or reradiated star light detected in the sub-millimeter (e.g. Blain et al. 1999). The longer wavelength tracers tend to find higher star formation densities, a result which has been attributed to dust absorption in the UV and optical (Calzetti & Heckman 1999; Meurer et al. 1997; Pettini et al. 1998).

The issue of the effects of dust on the evolutionary cycle associated with the optical Butcher-Oemler effect has been disregarded by most investigations to date. However, the recent analysis of the spectral catalog for the MORPHS sample (D99) by Poggianti et al. (1999, P99) has uncovered evidence for dust obscuration in at least one spectral class – e(a) galaxies. These galaxies have detectable [OII] emission and relatively strong Balmer absorption ($\text{EW}(\text{H}\delta) \geq 4$). These spectral features, along with other properties of the galaxies and of similar spectrally-classified local systems (P99; Poggianti & Wu 1999), were interpreted by P99 as probably arising from a dust-obscured starburst, with the [OII] line strength suppressed by dust absorption. The e(a) class is naturally identified as the progenitor of the large population of post-starburst galaxies in the clusters.

To obtain a complete view of the star formation properties of cluster galaxies free from the effects of dust obscuration we need to complement the optical studies with observations at longer wavelengths, from the near-infrared to the sub-mm and radio. In particular, observations in the sub-mm and far-infrared can trace the amount of star light absorbed by dust and reradiated at longer wavelengths. For the most extreme starburst galaxies in the local Universe this reradiated emission dominates the bolometric luminosity of the galaxies (e.g. Sanders & Mirabel 1996). Unfortunately, current sub-mm and far-infrared surveys lack the sensitivity to study all but the most extreme starburst galaxies ($\dot{M} \gtrsim 100M_{\odot} \text{ yr}^{-1}$) at moderate and high redshift. However, at radio wavelengths, the synchotron radiation from electrons accelerated by supernovae leads to a tight correlation between the radio and far-infrared fluxes of star-forming galaxies across a wide range in luminosity (Condon 1992). This means that in the absence of a radio-loud active nucleus the radio flux of a star-forming galaxy can be used to estimate its current massive star formation rate.

By employing the huge collecting area of the VLA we can undertake a sensitive radio survey for star formation in obscured galaxies down to limits of $\dot{M} \sim 5-10M_{\odot} \text{ yr}^{-1}$ at $z \sim 0.5$. To this end the VLA has been used in an ambitious survey to determine the evolution of the radio populations in a sample of very-rich clusters out to $z = 0.4$ (Morrison et al. 1999). The survey contains 14 clusters at $z = 0.10-0.18$, 12 more between $z = 0.20-0.25$ and a further four at higher redshifts, $z = 0.38-0.41$ (the radio observations discussed in this paper are of the most distant cluster in this survey). Morrison et al. (1999) find that the population of radio galaxies with luminosities above $2 \times 10^{22} \text{ W Hz}^{-1}$ in the most extreme clusters has increased by a factor of $\sim 5-6$ out to $z = 0.4$. They conclude that the radio galaxy population in very rich clusters has evolved significantly over the last 5 Gyrs.

In this paper we report on high resolution near-infrared

imaging from *HST* and sensitive radio observations with the VLA of a small field in the core of the distant cluster Cl0939+4713 (A 851, $z = 0.41$) for which high-resolution optical *HST* images and extensive archival spectroscopic observations are available. We combine these datasets to study the characteristics of galaxies in distant clusters and to search for the signatures of dust obscuration on their apparent properties.

In §2 we describe the *HST* optical and near-infrared imaging as well as the deep VLA 1.4-GHz map of this field. In §3 we then present our results on the properties of the radio-selected galaxies within our *HST* field drawing on published spectroscopy. We discuss these in §4 and give our main conclusions in §5. Throughout this paper we use $H_{\odot} = 50 \text{ km s}^{-1} \text{ Mpc}^{-1}$ and a $\Omega_{\odot} = 1, \Lambda = 0$ cosmology. In this geometry $1''$ corresponds to 6.5 kpc at $z = 0.41$.

2. OBSERVATIONS

2.1. NICMOS Imaging

The near-infrared *NICMOS* observations of Cl0939+4713 discussed here were obtained with Camera 3 during the special campaign in January 1998. Due to the distortion of the *NICMOS* dewar the wide-field Camera 3 (field-of-view $51.2''$ square, sampling $0.20''$ per pixel) was not par-focal with the other instruments on-board *HST* and to allow the diffraction-limited operation of this camera a special campaign was organised during which the main telescope optics were refocused on the Camera 3 focal plane.

The observations comprise a mosaic of four pointings through the F160W filter covering a combined field of around $100'' \times 100''$. Each pointing consists of four individual exposures of 1215 s, each spatially offset by $1.1''$ on a square grid to remove bad pixels and reduce the effects of flatfield variations. The total integration time per pixel for the mosaic is thus 4.86 ks. The data were reduced in a standard manner using the *NICMOS* data pipeline (CANNICA) and the most recent calibration files taken from the archive. Any remaining features in the background were removed with the UNPEDESTAL software kindly provided by Dr. R. van der Marel which worked well, and the final mosaicing was achieved using IMCOMBINE in IRAF. The mosaic was photometrically calibrated to give magnitudes on the H_{160} Vega system. This image provides restframe J -band morphologies at a resolution of around 1.3 kpc for cluster members (Fig. 1).

To create a complete catalog of objects detected within the *NICMOS* mosaic we analysed the frame using the SExtractor image analysis package (Bertin & Arnouts 1996). We adopted detection criteria of a minimum area of $\geq 0.4 \text{ sq. arcsec}$ (10 pixels) above an $\mu_{160} = 24.0 \text{ mag arcsec}^{-2}$ isophote and using these we detect 303 sources brighter than the approximate 3σ point-source flux limit of $H_{160} = 23.5$.

2.2. Radio Data

The VLA observations of Cl0939+4713 were obtained in B configuration at 1.4 GHz between 1996 January 06–08. The total integration time of the map is 60.7 ks at an effective resolution of $5.0''$ (33 kpc at $z = 0.41$). The map was cleaned and analysed using AIPS. Details of this complex procedure are given in Morrison et al. (1999). The map

reaches a 1σ noise level of $9\mu\text{Jy beam}^{-1}$. We detect 10 sources above $27\mu\text{Jy}$ (3σ) within the field defined by the overlap region of our *NICMOS* F160W mosaic and *Wide Field and Planetary Camera 2 (WFPC2)* F702W exposures (see Fig. 1). All ten sources have bright optical/near-infrared counterparts in our *HST* images. The properties of these ten sources are discussed in §3. The positions, fluxes and restframe radio power (using the redshifts from Table 2 and assuming an $S \propto \nu^{-0.7}$ spectrum) are reported in Table 1. Unfortunately due to the modest resolution of the map only two sources, #122 and #296, appear to be resolved and then only marginally. The radio and optical/near-IR images are aligned to an rms accuracy of $0.4''$ using the 8 brightest radio sources in the *NICMOS* field.

The flux limit of the radio sample corresponds to a radio power of just $2 \times 10^{22} \text{ W Hz}^{-1}$ at the redshift of the cluster. Comparing this limit to those achieved by radio surveys of local clusters we note that Gavazzi & Boselli (1999) detect galaxies as faint as $3 \times 10^{20} \text{ W Hz}^{-1}$ in their analysis of the radio luminosity function in the Virgo cluster (a factor of roughly $100 \times$ closer to us than Cl0939+4713) using the NVSS 1.4 GHz survey (Condon et al. 1998).

2.3. *WFPC2* Imaging

These observations were obtained as part of the Early Release Observations during the Science Verification Phase after the installation of the *WFPC2* on board *HST*. The observations comprise a total of 21.0 ks of integration through the F702W filter (Dressler et al. 1994b). The exposures were dithered by integer pixels to allow the removal of defects and cosmic ray events. The position of the corrective optics within *WFPC2*, to correct for the aberration of the primary mirror, was not optimal during these observations and combined with a higher than ideal operating temperature for the CCDs these images are not as cosmetically clean as later exposures with *WFPC2*. Nevertheless, they provide deep ($R \sim 26$) imaging of the core of the cluster at $0.1\text{--}0.2''$ resolution in the restframe *B*-band.

The reduction and analysis of the F702W exposure of this field is described in more detail in Smail et al. (1997), who provide a complete catalog of objects detected in the field with photometry calibrated to the R_{702} passband described by Holtzman et al. (1995). Smail et al. (1997) also discuss visually classified morphologies on the revised Hubble scheme for the brighter galaxies within this field down to $R_{702} = 23.5$. There are a total of 123 galaxies with morphologies from S97 within the joint *NICMOS*/*WFPC2* field. All ten of the radio sources selected from the VLA map are included in the S97 catalog and we list the Hubble type for each galaxy in Table 2. We also give the Disturbance Index (D), which is a measure of how disturbed the galaxy seemed compared to the typical appearance of a galaxy with its Hubble type locally, where $D = 0$ is “normal” and $D = 4$ is highly disturbed (S97). In addition to these objective measures, a subjective interpretation of the source of the disturbance was also given by S97 and

is listed in the table (e.g. Chaotic, Tidal interaction, etc). We note in particular that a galaxy would be classed as “Merger” if two or more close nuclei were seen in a common envelope. These visual estimates were shown to correlate well with the machine-based asymmetry measurements (S97) and have been used to attempt to isolate and study the role of dynamical interactions in triggering the Butcher-Oemler effect (e.g. D99).

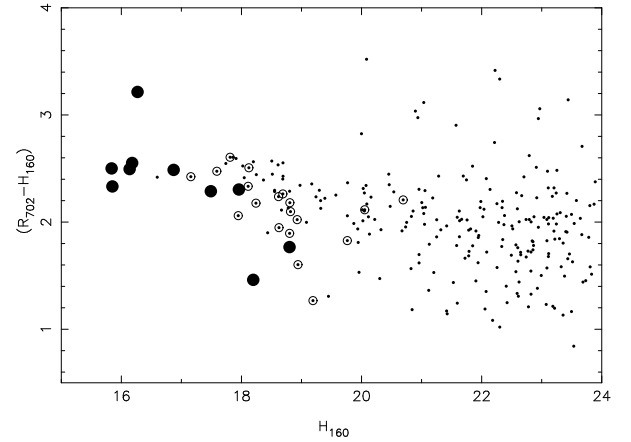


Fig. 2. The $(R_{702} - H_{160}) - H_{160}$ color-magnitude distribution for the sources lying in the joint *WFPC2/NICMOS* field. The $(R_{702} - H_{160})$ color is measured within an aperture of diameter 2.5 times the FWHM of the galaxy in the F160W image. The large filled points denote those galaxies detected in the VLA map, the circled points are other galaxies with spectroscopic identifications in D99 and the small points are the remaining sources selected from the F160W catalog. Note the sequence of red galaxies associated with early-type cluster members which extends down to $H_{160} \sim 23$.

To investigate the optical-infrared colors of the galaxies in our sample we have aligned and resampled the *WFPC2* image to the reference frame of the *NICMOS* exposure. A comparison of stars and compact galaxies in the resampled F702W exposure and the F160W image shows that they have very similar profiles in the two bands indicating that the resolution is dictated by the pixel sampling of the images. This suggests that PSF variations should not strongly influence our analysis. To confirm this we have convolved the *WFPC2* and *NICMOS* images with a model PSF for the other instrument generated using TINYTIM (Krist & Hook 1999). The colors determined from these convolved images show no systematic differences from those measured from the unsmoothed images and hence we use the latter in the following analysis.

To measure colors from our F702W and F160W exposures we have used the IRAF task PHOT and apertures matched to the near-infrared extent of the galaxies. The diameter of the photometry apertures were taken as 2.5 times the FWHM of each source from the F160W catalog (d_{phot} in Table 2). The color-magnitude diagram for the field is shown in Fig. 2, with the radio sources and spectroscopically identified galaxies marked. We give total H_{160} magnitudes and aperture $(R_{702} - H_{160})$ colors for the ten radio sources in Table 2.⁷ We show the F160W and F702W images of this sample in Fig. 3.

To study the color variations within the galaxies we have

⁷For interest we list here the $(R_{702} - H_{160})$ colors of the various $z > 3$ lensed galaxies identified by Trager et al. (1997). These galaxies are all relatively blue compared to the general field (Fig. 2), $(R_{702} - H_{160}) = 1.25 \pm 0.10$ for DG#334 at $z = 3.34$, $(R_{702} - H_{160}) = 0.78 \pm 0.15$ for the $z = 3.97$ source seen as P1/P2/P3 and $(R_{702} - H_{160}) = 1.43 \pm 0.20$ for the $z = 3.98$ arclet A0, although this may suffer contamination from the nearby bright cluster galaxy (#426, Fig. 3). A search of the *NICMOS* and *WFPC2* images to identify galaxies with extreme colors turned up a very red disk galaxy near the center of the field: #333 (Fig. 1), this is the reddest, bright object in the field with $H_{160} = 19.53$ and $(R_{702} - H_{160}) = 5.4 \pm 0.2$ (c.f. Treu et al. 1999).

TABLE 1
PROPERTIES OF THE RADIO GALAXY SAMPLE

Source ID	R.A. (J2000)	Dec.	$S_{1.4}$ (μ Jy)	$P_{1.4}$ (10^{22} W Hz $^{-1}$)	Comments
36	09 42 58.16	+46 59 53.4	79 \pm 9	5.9	
122	09 42 57.62	+46 59 45.3	204 \pm 9	15.2	Resolved?
224	09 42 55.80	+46 59 40.4	55 \pm 9	4.0	
230	09 43 02.32	+46 59 28.7	52 \pm 9	3.8	$P_{1.4}$ assumes $z = 0.41$
296	09 43 02.81	+46 59 24.2	644 \pm 9	47.6	Resolved?
399	09 42 57.84	+46 59 13.3	43 \pm 9	3.1	
426	09 42 56.21	+46 59 12.0	32 \pm 9	2.4	
536	09 43 00.03	+46 58 53.4	196 \pm 9	14.5	
610	09 42 57.34	+46 58 50.4	158 \pm 9	11.7	
640	09 42 55.08	+46 58 41.7	57 \pm 9	2.6	

constructed F702W–F160W color images for each galaxy in our spectroscopic sample. We show the color images for the relevant radio-detected galaxies in Fig. 3 to illustrate the internal color variations within these galaxies. A comparison sample of confirmed cluster members which are not detected in the radio map is shown in Fig. 4. We note that PSF-convolved versions of these images are qualitatively similar, in particular the blue cores at the centers of #296, #399 and #426 do not appear to result from differences in the PSF between the two passbands.

2.4. Spectral Information

Spectroscopic observations of galaxies within our field are available from the MORPHS spectral catalog (D99). The targets for these observations were selected from the F702W exposure and D99 amassed spectra for 28 galaxies within the *NICMOS* field, comprising 22 cluster members and 6 field galaxies. These spectra typically cover the spectral region from 3000–6000Å in the restframe, including any [OII] λ 3727 emission but in most cases not H α . The galaxies have all been classified using the spectral classification scheme of D99 as follows: passive galaxies (k); post-starburst (k+a/a+k), these show no [OII] and strong Balmer absorption indicative of a cessation of star formation within the last Gyr or so; actively star forming (e(c)/e(b)/e(a)), e(c) have spectral properties similar to local spiral galaxies, e(b) have stronger [OII] and are interpreted as starburst galaxies, e(a) have moderate [OII] but stronger Balmer lines than e(c) galaxies. The e(a) class has been interpreted as dusty starbursts (P99) where the [OII] is suppressed by dust within the galaxy (supported by the observations of anomalously high H α /[OII] ratios for these galaxies, see also §1). The distribution of cluster/field galaxies in the different spectroscopic classes is: k (7/2); k+a (6/0); a+k (2/0); e(a) (5/1); e(b) (1/0); e(c) (2/1). The spectrum of one field galaxy has too low signal-to-noise to allow a reliable classification.

For the ten radio sources in the field, spectra and spectral classifications are available from D99 for nine galaxies (galaxy #230 lacks a spectroscopic ID) and we list these in Table 2. Of these nine galaxies, eight are cluster members and one is a field galaxy (the Sab galaxy #640).

3. RESULTS

⁸We note that the radio population has similar dynamics to those cluster members undetected in the radio map: we calculate a restframe velocity dispersion of $\sigma = (960 \pm 160)$ km s $^{-1}$ for the eight radio-detected members compared to $\sigma = (1110 \pm 140)$ km s $^{-1}$ for the 12 undetected members lying within the same field.

With a small sample of galaxies our conclusions are by necessity fairly qualitative in nature and this paper should be seen as the prelude to the analysis of a larger sample of radio-selected galaxies in distant clusters by Morrison et al. (1999). Nevertheless, we will use our observations, and particularly the high resolution near-infrared imaging with *NICMOS*, to illustrate the general characteristics of radio galaxies in distant clusters and to emphasise the effects of dust in galaxies on their perceived properties.

3.1. Radio-selected Sample

We have detected ten galaxies above the 3σ flux limit ($S_{1.4} \geq 27\mu$ Jy) of the VLA map which lie within the joint *NICMOS*/*WFPC2* field. The spectroscopic information available from D99 allows us to identify eight of these galaxies as cluster members (or 35% of the 22 cluster galaxies known within this field) and a further source as a foreground field galaxy (12% of the spectroscopically-confirmed field population within our image). Our field size corresponds to a region $\sim 650 \times 650$ kpc in extent at the cluster redshift and the equivalent radio power limit is 2×10^{22} W Hz $^{-1}$. A comparably deep survey of a similar region in the core of a rich local cluster would typically detect $\lesssim 1$ galaxy (e.g. Fig. 5), compared to the eight detected here. This suggests a substantial increase in the rate of occurrence of radio sources in high density environments at moderate redshifts (Morrison et al. 1999).

The galaxies included in the radio-selected sample of cluster members are typically the brighter galaxies in our field (Fig. 2), including the brightest four galaxies (in the restframe *B*-band). The whole sample spans a range of magnitudes $R_{702} = 18.3$ – 20.8 ($L_B \sim 4$ – $0.4L_B^*$). The colors of the fainter radio-detected galaxies are slightly bluer than equivalently luminous, undetected cluster members, with the brighter radio-emitting galaxies having comparable (red) colors to the undetected population (Fig. 2). The fact that we only detect the optically brightest galaxies in the radio map may suggest that the majority of cluster galaxies would be detected if we could increase the sensitivity of the radio observations by a factor of a few (see Fig. 5).⁸

In our analysis we will assume that the local relationship between star formation rate and radio emission (e.g. Condon 1992) holds for spiral galaxies detected in distant clusters. The validity of the local relationship at least

TABLE 2
OPTICAL/NEAR-INFRARED PROPERTIES OF THE RADIO SAMPLE

Source ID	z	H_{160}	$(R_{702} - H_{160})$	d_{phot} ('')	Morph. Type	Spectral Type	$\text{EW}(\text{H}\delta)$ (Å)	D	Comments
36	0.4119	18.20	1.46 ± 0.10	5.6	Sd	e(a)	10.2	2	EW([OII]) = -6.9\AA ; Merger
122	0.4125	17.96	2.30 ± 0.10	2.7	Sd	a+k	11.6	3	Merger, $\text{H}\delta$ measurement uncertain.
224	0.4076	15.85	2.33 ± 0.04	5.8	Scd?	k+a	6.1	2	Merger
230	...	18.80	1.77 ± 0.14	2.2	Irr	2	no spectrum in D99
296	0.4014	16.87	2.49 ± 0.07	2.5	E	k+a	4.6	0	
399	0.4109	16.14	2.50 ± 0.05	2.5	E	k	0.0	0	
426	0.4037	16.18	2.55 ± 0.05	3.9	E	k	0.0	0	
536	0.4111	17.49	2.29 ± 0.08	4.0	Sc	a+k	8.6	3	Tidal?
610	0.4007	15.84	2.50 ± 0.05	3.4	Sa/S0	k+a	4.2	1	Merger?
640	0.3324	16.27	3.21 ± 0.04	8.3	Sab	k:	0.0	1	Field galaxy, low s/n spectrum — possible e(a)?

for the distant field appears to be supported by recent observations (Georgakakis et al. 1999). However, we caution that the exact star formation rates derived from this analysis may have substantial systematic uncertainties. In particular the claim that the radio to far-infrared correlation varies locally between galaxies in rich clusters and those in the field (Andersen & Owen 1995) may indicate an environmental influence in the conversion from radio luminosity to star formation rate (SFR) resulting from the compression of the galactic magnetic field by the galaxy's motion through the intracluster medium (ICM). Without a fuller understanding of the state of the ICM in distant clusters it is difficult to quantify the extent of this bias on the radio-derived SFRs of distant cluster galaxies. We have chosen therefore to quote the SFRs determined using the local field relationship and the correction which should be applied if the radio population in distant clusters shows the same behaviour as is claimed for galaxies in rich clusters locally.

3.2. Optical Morphologies

Turning to the restframe B -band morphologies of the radio sources (Table 2 & Fig. 3) we see that they fall roughly equally into two broad classes: optically-luminous early-type galaxies (E and S0/Sa) and mid- to late-type spiral galaxies (Sc–Sd/Irr).

In their analysis of galaxies in the Virgo cluster detected in the NVSS radio survey, Gavazzi & Boselli (1999) found that the most powerful radio sources in spirals were also in mid-type, Sb–Sc, systems. To compare the optical and radio properties of the galaxies we plot the 1.4-GHz restframe power versus the optical B -band luminosity for all spectroscopically-confirmed members in Fig. 5, separated into early- and late-type. The early-type galaxies show a wider range in their $P_{1.4}/M_B$ values than the spirals, but span a similar region of the $P_{1.4}-M_B$ plane as radio-selected E/S0 galaxies in the Virgo cluster (Fig. 5). This is as expected if the radio emission from the early-type galaxies is coming from a central AGN. In contrast the radio emission from the spirals is (by analogy to local systems) most likely synchotron emission associated with active star formation and leading to a correlation between the radio power and the optical luminosity of the galaxy. We note that the population of radio-emitting spiral galaxies identified by Gavazzi & Boselli (1999) in Virgo have radio powers 5× lower at a fixed B -band luminosity than the galaxies we are detecting in Cl0939+4713 (Fig. 5).

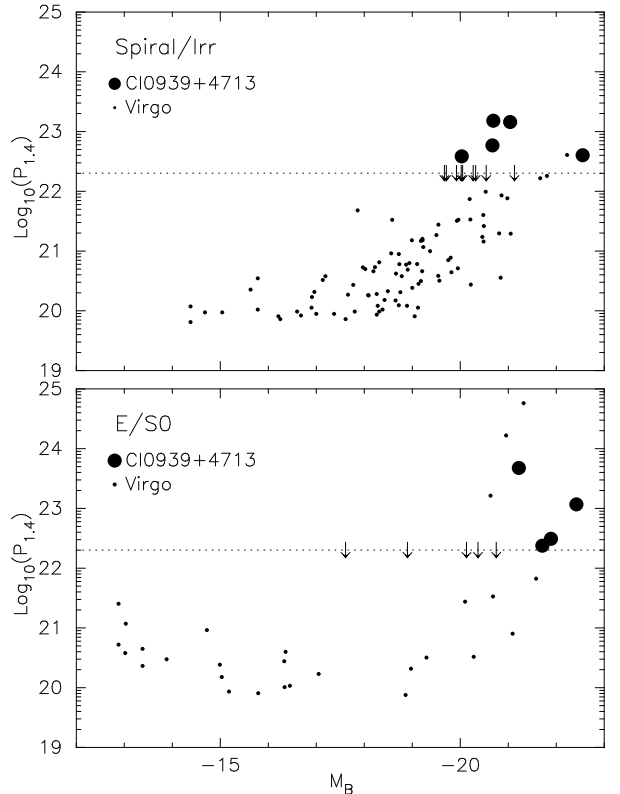


Fig. 5. The $P_{1.4}-M_B$ distribution for those galaxies detected in the VLA map of Cl0939+4713 compared to the equivalent distribution for the Virgo cluster (Gavazzi & Boselli 1999). The top panel compares the distributions for the morphologically-classified spiral and irregular galaxies in both clusters, while the lower panel shows the equivalent comparison for elliptical and S0 members. We adopt an apparent magnitude of $R_{702} = 19.7$ for an $M_B = -21.1$ (L_B^*) galaxy in the R_{702} -band observed at $z = 0.41$ (assuming an SED typical of a present-day Sbc galaxy). The dotted lines show the radio flux limit of our sample in Cl0939+4713. We indicate the spectroscopically-confirmed member galaxies which are undetected in the VLA map as upper limits.

The association of around 60% of the bright radio-selected sample with spiral galaxies suggests that the evolution in the radio populations within clusters runs in parallel to the increasing fraction of blue star-forming galaxies found in these regions at $z \gtrsim 0.2$, the Butcher-Oemler effect. The rise in the fraction of bright spiral galaxies in clusters such as Cl0939+4713 is a factor of ~ 5 out to $z = 0.4$ (Dressler et al. 1997). Even without the increased radio luminosity of the brightest cluster spiral galaxies, this increase in the proportion of spirals is enough to explain the evolution in the number of radio sources seen

in the distant clusters (a factor of ~ 5 –6, Morrison et al. 1999). The increase in the spiral fraction in the clusters is believed to result from infall from the surrounding field associated with the growth of the clusters. A rise in the radio activity of moderate redshift field galaxies has also been observed and attributed to star formation in these galaxies (Georgakakis et al. 1999). However, to fully understand the evolution of the radio population in the cluster we also need to identify the cause of the increased radio luminosities of the bright spiral galaxies. We note that our use of a local cluster sample in the comparison should minimise the possible environmental effects which could explain this apparent brightening, and moreover the increase in radio luminosities is substantially above that claimed to result from environmental effects within local clusters (§3.1).

3.3. Near-infrared Morphologies

We now discuss the internal structure of the cluster galaxies in our *HST* images (Fig. 3 and 4) and the important insights which our *NICMOS* near-infrared imaging has provided into the nature of these systems. Starting with the early-type galaxies we see relatively uniform optical-near-infrared colors (as shown by their lack of structure in the F702W–F160W images in Fig. 3 and 4). A few contain blue cores, which may be associated with central AGN, although the details of these features are sensitive to the exact form of the PSF in the F702W and F160W images and so we do not discuss them further here.

A comparison of the F702W and F160W morphologies for the late-type radio sources in Fig. 3 shows that in these systems there are substantial differences in the appearance of these galaxies between the restframe *B*- and *J*-bands. The near-infrared morphologies are considerably more relaxed and symmetrical. However, the lack of a morphological classification scheme for local galaxies based on near-infrared imaging means that is not useful to attempt to reclassify the galaxies on the basis of the F160W images.

More interestingly, the F702W–F160W images in Fig. 3 show that in a large number of cases the irregular structures seen in the rest-frame *B*-band within the central regions of the late-type galaxies are replaced by a much more regular appearance in the near-infrared and so must be due to very red structures (visible as white regions in Fig. 3). These features are substantially redder than the outskirts of the galaxies (up to $\Delta(R-H) \sim 1.3$ –1.5) and could represent differences in the stellar populations within the galaxies or simply dust obscuration. To distinguish between these alternatives we concentrate on the large fraction of galaxies whose integrated spectra show post-starburst stellar populations. The lack of emission lines in the optical spectra indicates that there is no visible star-formation in the outskirts of these galaxies, which also show the red optical-infrared colors typical of an evolved stellar population (see the integrated colors in Fig. 2). In this situation it is very difficult to make the stellar population in the central regions of the galaxies substantially redder than the outskirts without invoking a contrived scenario. In contrast, dust obscuration can easily produce both the apparently red colors and its structured distribution. We propose therefore that large quantities of dust are probably a common feature of these galaxies.

The small scale features seen in the optical images of

these galaxies which we claim are due to dust obscuration have been previously interpreted as arising from dynamical disturbance of these galaxies, suggesting a dynamical origin for their star formation activity (S97). To understand the consequences of this change in interpretation of these galaxies we focus on those galaxies classified in the optical as showing signs of morphological disturbance by S97. There are a total of eight spectroscopically confirmed members in our sample with disturbance indices of $D \geq 2$ indicating abnormally disturbed morphologies, all of these are disk galaxies and they are typically classified as mergers or tidally disturbed, half of them are detected in our radio map. These galaxies exhibit substantially more regular morphologies in the near-infrared (Figs. 3 & 4), in particular the apparently double structures seen in the F702W morphologies of the radio sources #36, #122 and #536 all disappear in the F160W passband.

We also see signs of dust obscuration in the disturbed galaxies which are not radio sources (#171, #369, #497 and #622), although arguably not as extreme as the radio-selected sample. In a few cases there are other signatures of interactions in the F702W images apart from double nuclei, etc, such as low-surface brightness tidal features or companion galaxies (e.g. #224 or #497), which indicate that these are true merging or interacting systems. But, in the majority of the galaxies their high disturbance index was based upon the apparent presence of multiple nuclei in the central regions of the galaxies (see §1). We suggest that in fact dust obscuration is the correct explanation for their irregular appearance in the restframe *B*-band which results in their classification as disturbed or merging. We estimate that of the eight confirmed members with $D \geq 2$ based on the F702W imaging, at least half (#36, #122, #171, #622) would have $D < 2$ if classified from the F160W images, suggesting that the occurrence of highly disturbed galaxies in the core of Cl0939+4713 may have been overestimated by up to a factor of two.

We conclude from our comparison of the near-infrared and optical morphologies of a small sample of confirmed cluster members that the frequency of galaxies showing small-scale signatures of disturbance or interaction is probably substantially less than has been suggested from optical studies (e.g. S97) due to obscuration by dust. This effect acts in addition to the standard luminosity bias in optically-selected samples towards actively star-forming galaxies (the usual justification given for undertaking near-infrared surveys of distant clusters, e.g. Barger et al. 1996). The expectation of previous optically-based studies was that dust obscuration would not be a significant bias when comparing the distant morphological samples with more local examples as they were comparing effective restframe *B*-band observations in both cases (S97). However, this expectation seems to have been misleading due to the wider prevalence of dust in cluster galaxies at $z \sim 0.4$, perhaps associated with the increased activity in galaxies at these epochs.

3.4. Spectral Properties

Looking now at the spectral properties of the radio-selected cluster members we see something striking: five of the galaxies have spectral features which class them as post-starburst (a+k/k+a) systems using the scheme of P99 (Table 2). Moreover, these five radio sources show

the strongest Balmer absorption lines of the eight post-starburst galaxies in our cluster sample (they are also the brightest five post-starburst galaxies). There are no post-starburst field galaxies in our sample.

The detection of post-starburst galaxies in the radio waveband is surprising. These galaxies are selected to have no detectable [OII] emission and hence are expected to have no on-going massive star formation (observations of the spectral region including any H α emission in these galaxies would make this statement more robust). In contrast, the radio emission is most easily explained as arising from massive star formation (although some contribution from an obscured radio-loud AGN cannot be ruled out with our present data). The expected lifetime of the radio emission after the starburst is $\ll 0.1$ Gyr, thus if they are post-starburst systems these galaxies must all be seen *just* after the cessation of their star formation. This seems very unlikely as the length of time in which the post-starburst signature (strong H δ absorption) is visible is ~ 1 Gyr and we would thus expect to see an order of magnitude more radio-quiet k+a galaxies, where the radio emission had decayed but the Balmer absorption is still visible. This population is not observed. Therefore, we conclude that massive stars are currently being formed in these galaxies.

Where is the site of the active star formation in the a+k/k+a cluster galaxies? The optical spectra typically sample the whole of the bulge and disk of the galaxy (see D99) and thus it is unlikely that we are missing emission from the outskirts of the galaxy. We suggest instead that the star formation is occurring in the central regions of these galaxies but is hidden from view by the dust which we see there in our F702W–F160W images. This possibility was raised in P99 who stated that the most extreme e(a) galaxies might appear as post-starburst systems (a+k/k+a) due to obscuration of the emission regions. The reddened regions lie in the central 5–10 kpc of the galaxies (Fig. 3 & 4) and have optical–near-infrared colors which are typically $\Delta(R_{702} - H_{160}) \sim 1$ magnitude redder than the outskirts of the galaxies. This would indicate optical extinctions of at least $A_B \sim 2$ mag to the population of disk stars (let alone the active sites of star formation) although this estimate is highly uncertain due to resolution effects.

Four of the five radio-selected post-starburst galaxies are disk galaxies and we can estimate their star formation rates (SFR) from their radio power using the calibration of Condon (1992). We find that these galaxies are typically forming massive stars ($M \geq 5M_\odot$) at rates of $\sim 10 M_\odot \text{ yr}^{-1}$, with the highest SFRs being $30 M_\odot \text{ yr}^{-1}$ for #122 and #536. This assumes no boosting of the radio emission due to compression of the galactic magnetic fields by the cluster ICM, which could amount to a factor of ~ 2 (Andersen & Owen 1995). Combining these SFRs with the B -band luminosities of the galaxies we can predict their [OII] fluxes if the star formation regions are unobscured using the relations given in Kennicutt (1992). We can then roughly estimate the amount of extinction needed for this line to be undetected in the optical spectra, $\text{EW}([\text{OII}]) \lesssim 5 \text{\AA}$. We find that the star forming regions would need to suffer $A_B \gtrsim 3$ mag of extinction for the [OII] line to be undetected in the D99 spectra ($A_B \gtrsim 2$ mag if we assume the radio fluxes are artificially raised). This amount of obscuration is not unreasonable given the ex-

tent of the dust reddening seen in the F702–F160W images (Figs. 3 & 4). We note that if we assume this dust is cold, $T_D \sim 40$ K, then the predicted sub-mm fluxes of these galaxies will be only $S_{850} \sim 0.5 \text{ mJy}$ at $850 \mu\text{m}$. This is well below the confusion limit of current sub-mm instrumentation in blank fields.

There are also examples of proposed dusty galaxies within our sample which are not detected in the radio map. In particular three of the cluster galaxies have e(a) spectral features and evidence for dust in their F702–F160W images (Fig. 4, #177, #369 and #622). These galaxies are optically fainter than the e(a) galaxy which is detected in the radio, #36, and it is possible that their lower overall luminosities mean that their radio emission is below the limit of the VLA map. Interestingly, although the e(a) spectral class was interpreted as dusty starbursts in P99, the radio map places upper limits on the current rate of massive star formation in the undetected e(a) galaxies of $\dot{M} \lesssim 5M_\odot \text{ yr}^{-1}$, with similar limits applying to the galaxies with e(c) spectra in the field (e.g. #165 and #497 in Fig. 4). Taking the possible boosting of the radio emission due to compression of the galactic magnetic fields by the cluster ICM (§3.1) into account these SFR limits could be dropped by a factor of two or more.

4. DISCUSSION

We see a combination of post-starburst spectral features, radio emission and apparently large quantities of dust within the spiral galaxies in our sample. These characteristics can be most easily accommodated if they exist in spatially distinct regions of the galaxies, as suggested by our color maps. The radio emission would arise from massive star formation in the dust obscured center of the galaxy, while the A stars trace the remnants of an earlier ($\lesssim 1$ Gyr) strong star formation episode within the galactic disk. There is weak evidence in our sample for a correlation between H δ line strength and radio luminosity which would suggest that there is a causal link between the numbers of A stars and the current (obscured) star formation rate, probably as a result of a single triggering mechanism.

This triggering mechanism could be a cluster-related phenomenon, a view which is supported by the lack of obvious post-starburst systems in samples of faint radio sources in the field (Hammer et al. 1995; L.L. Cowie, priv. comm.). Thus, we may be seeing a more dynamic situation including cluster-driven processes, whereby interactions between the intracluster medium and the cold molecular gas within the galactic disks accelerates the collapse and evaporation of the star forming regions. The effects of the ICM on the galactic disk are expected to be a function of the local density in the disk – with lower density regions in the outskirts of the disks being most severely effected, while star formation continues almost unaffected in the inner regions of the galaxy. Thus environmental processes could result in a combination of post-starburst and starburst within individual cluster galaxies. Studies of the spatial distribution and kinematics of larger samples of radio-selected galaxies may be able to discriminate between the different physical processes which could be operating (Morrison et al. 1999).

Alternatively, perhaps this activity may be triggered by a more general physical process, unrelated to the cluster environment. Indeed, similar behaviour is seen in

the models of interacting field galaxies published by Mihos & Hernquist (1996) (although we have argued that a substantial fraction of apparently disturbed cluster spiral galaxies probably arise from dust obscuration, rather than true interactions). For a range of models for tidal interactions between galaxies Mihos & Hernquist predict that spatially-extended enhanced star formation will first occur in the disk of the galaxy. This is followed on a timescale of a $\sim 0.1\text{--}0.3$ Gyr by funnelling of any remaining gas into the center of the galaxy where it reaches very high densities and triggers an (obscured?) nuclear starburst. Again, more detailed investigation of the kinematics and internal dynamics of these galaxies may provide useful diagnostics to distinguish between the competing models.

The picture which is appearing is one in which galaxies which are visibly forming stars appear to have modest star formation rates, $\lesssim 5M_{\odot} \text{ yr}^{-1}$ ($M \geq 5M_{\odot}$), while more vigorous star formation, $\gtrsim 10\text{--}30M_{\odot} \text{ yr}^{-1}$ is on-going in highly obscured regions in the centers of what appear to be post-starburst galaxies. If the radio fluxes of these distant galaxies are increased by the same environmental effects which are claimed to boost the radio emission of local cluster galaxies and to the same extent (Andersen & Owen 1995) then the quoted SFRs should be reduced by a factor of ~ 2 . Sensitive observations to search for H α emission (or emission lines further into the near-infrared) will provide a stronger test of the star formation rates in these galaxies, the extent of obscuration within them and the degree to which their radio emission deviates from that seen in the distant field population due to environmental processes. Finally we note that by having post-starburst and starburst phases occurring in parallel within a single galaxy it is possible to reduce the high fraction of galaxies ($\sim 100\%$, Barger et al. 1996) which must pass through this phase to explain the large numbers of post-starburst systems seen within distant clusters (Barger et al. 1996; P99).

5. CONCLUSIONS

In summary, we have highlighted the role that dust plays in obscuring our view of the morphologies and star formation properties of distant galaxies. We have shown that selection at faint radio fluxes provides a powerful technique for identifying spectrally-classified post-starburst and starburst galaxies crucial to our understanding of the evolutionary cycle of galaxies in clusters (e.g. P99). Using this new tool we can undertake statistical studies to search for the mechanism responsible for triggering and/or quenching of this activity (P99; Morrison et al. 1999). The main conclusions of our study are:

- We present optical and near-infrared imaging with *HST* of a region in the core of the distant rich cluster Cl0939+4713 at $z = 0.41$.
- We compare the high resolution near-infrared and optical morphologies of a sample of 22 cluster members. This shows that while the broad morphological classifications are similar, the frequency of galaxies showing small-scale signatures of disturbance or interaction is substantially less when using the near-infrared imaging. We suggest that obscuration by dust has led optical studies to conclude that an anomalously high fraction of galaxies have suffered small scale disturbances. This may point to a wider prevalence of dust in cluster galaxies at $z \sim 0.4$, perhaps

as a result of the increased star formation activity at these epochs.

- Using a very deep VLA 1.4-GHz map of this area we select a sample of ten radio galaxies in our field above a flux limit of $S_{1.4} = 27\mu\text{Jy}$, equivalent to a restframe 1.4-GHz power of $2 \times 10^{22} \text{ W Hz}$ at the cluster redshift. The faint radio sources are associated with two populations of cluster galaxies: luminous early-type galaxies, the radio emission from these galaxies originates from AGN; and dusty galaxies with late-type spiral morphologies, the radio emission here is expected to trace massive star formation (although the exact relationship between the radio luminosity and the SFR is uncertain due to environmental influences).
- The optical spectral characteristics of the late-type radio members are highly unusual – they appear to be post-starburst systems. We suggest that these galaxies are not post-starburst but in fact host highly obscured star-formation and starbursts. This is supported by our high resolution optical–near-infrared imaging which shows that the central regions of these galaxies are heavily dust enshrouded. If they continued for several 100 Myrs, these dust enshrouded nuclear-starbursts could build a substantial stellar bulge in the remnant of these luminous disk galaxies, possibly contributing to the formation of the S0 population in the clusters (Mihos & Hernquist 1996).
- We emphasise that a lack of consideration of the effects of dust on the morphological and spectral properties of galaxies, even at the relatively modest redshifts discussed here, may lead to an incomplete understanding of the cycle of star formation in cluster galaxies. Further work on this subject is urgently required.
- This paper is the prelude to a larger study of the *HST* morphologies and spectral properties of radio-selected galaxies in Cl0939+4713 and other high redshift clusters (Morrison et al. 1999). We expect that extensive studies with higher spatial resolution and wider wavelength coverage in the near future using the upgraded VLA and the next generation of millimeter interferometers will provide new insights into the prevalence and distribution of dust in distant galaxies.

ACKNOWLEDGEMENTS

This paper is based upon observations obtained with the NASA/ESA *Hubble Space Telescope* which is operated by STSCI for the Association of Universities for Research in Astronomy, Inc., under NASA contract NAS5-26555 and on observations from the Very Large Array which is operated by Associated Universities, Inc., under a cooperative agreement with the National Science Foundation. We thank Lisa Storrie-Lombardi and Lin Yan for help with *NICMOS* photometry and Giuseppe Gavazzi and Alessandro Boselli for kindly providing the data on radio galaxies in Virgo in electronic form. We also thank John Hill and the *NICMOS* GTO team for allowing us to observe this target. We acknowledge the use of the Pedestal Estimation and Quadrant Equalization Software developed by Roeland P. van der Marel. We thank an anonymous referee for detailed comments on this work and Amy Barger, Andrew Blain, Warrick Couch, Len Cowie, Alan Dressler, Alastair Edge, Gus Oemler and especially Bianca Poggianti for useful conversations. IRS acknowledges support from the Royal Society and RJI from PPARC.

REFERENCES

Abraham, R.G., Smecker-Hane, T.A., Hutchings, J.B., Carlberg, R.G., Yee, H.K.C., Ellingson, E., Morris, S., Oke, J.B., Rigler, M., 1996, *ApJ*, 471, 694

Andersen, V., Owen, F.N., 1995, *AJ*, 109, 1582

Balogh, M.L., Morris, S.L., Yee, H.K.C., Carlberg, R.G., Ellingson, E., 1999, *ApJ*, submitted

Barger, A.J., Cowie, L.L., Sanders, D.B., Fulton, E., Taniguchi, Y., Sato, Y., Kawara, K., Okuda, H. 1998, *Nature*, 394, 248

Bertin, E., Arnouts, S., 1996, *A&A*, 117, 393

Blain, A.W., Kneib, J.-P., Ivison, R.J., Smail, I., 1999, *ApJ*, 512, L87

Butcher, H., Oemler, A. Jr., 1984, *ApJ*, 285, 426

Calzetti, D., Heckman, T.M., 1999, *ApJ*, in press

Condon, J., 1992, *ARA&A*, 30, 575

Condon, J., et al., 1998, *AJ*, 115, 1693

Couch, W.J., Ellis, R.S., Sharples, R.M., Smail, I., 1994, *ApJ*, 430, 121

Couch W.J., Barger A.J., Smail, I., Ellis R.S., Sharples R.M., 1998, *ApJ*, 497, 188

Couch W.J., Sharples R.M., 1987, *MNRAS*, 229, 423

Dressler A., Gunn J.E., 1992, *ApJS*, 78, 1

Dressler, A., Oemler, A. Jr., Butcher, H., Gunn, J.E., 1994a, *ApJ*, 430, 107

Dressler, A., Oemler, A. Jr., Sparks, W.B., Lucas, R.A., 1994b, *ApJ*, 435, L23

Dressler, A., Oemler, A. Jr., Couch, W.J., Smail, I., Ellis, R.S., Barger, A., Butcher, H., Poggianti, B.M., Sharples, R.M., 1997, *ApJ*, 490, 577

Dressler, A., Smail, I., Poggianti, B.M., Butcher, H., Couch, W.J., Ellis, R.S., Oemler, A. Jr., 1999, *ApJS*, in press (D99)

Fabricant, D.G., Bautz, M.W., McClintock, J.E., 1994, *AJ*, 107, 8

Fabricant, D.G., et al., 1999, in prep

Fisher, D., Fabricant, D., Franx, M., van Dokkum, P., 1998, *ApJ*, 498, 195

Gavazzi, G., Boselli, A., 1999, *A&A*, 343, 93

Georgakakis, A., Mobasher, B., Cram, L., Hopkins, A., Lidman, C., Rowan-Robinson, M., 1999, *MNRAS*, in press

Hammer, F., Crampton, D., Lilly, S.J., Le Fèvre, O., Kenet, T., 1995, *MNRAS*, 276, 1085

Holtzman, J.A., Burrows, C.J., Casertano, S., Hester, J.J., Trauger, J.T., Watson, A.N., Worthey, G., 1995, *PASP*, 107, 1065

Kennicutt, R.C., 1992, *ApJ*, 388, 310

Krist, J., Hook, R., 1999, Tiny Tim v4.4, <http://scivax.stsci.edu/~krist/tinytim.html>

Lavery, R.J., Henry, J.P., 1988, *ApJ*, 330, 596

Lavery, R.J., Pierce, M.J., McClure, R.D., 1992, *AJ*, 104, 2067

Lilly, S.J., Le Fevre, O., Hammer, F., Crampton, D., 1996, *ApJ*, 460, L1

Meurer, G.R., Heckman, T.M., Lehnert, M.D., Leitherer, C., Lowenthal, J., 1997, *AJ*, 114, 55

Moore, B.E., Lake, G., Katz, N., 1998, *ApJ*, 495, 139

Morrison, G., Owen, F.N., et al., 1999, in prep.

Mihos, J.C., Hernquist, L., 1996, *ApJ*, 464, 641

Oemler, A. Jr., Dressler, A., Butcher, H., 1997, *ApJ*, 474, 561

Pettini, M., Kellogg, M., Steidel, C.C., Dickinson, M.E., Adelberger, K.L., Giavalisco, M., 1998, *ApJ*, 508, 539

Poggianti, B.M., Smail, I., Dressler, A., Couch, W.J., Barger, A.J., Butcher, H., Ellis, R.S., Oemler, A. Jr., 1999, *ApJ*, in press (P99)

Poggianti, B.M., Wu, H., 1999, in prep

Sanders, D.B., Mirabel, I.F., 1996, *ARA&A*, 34, 749

Smail, I., Dressler, A., Couch, W.J., Ellis, R.S., Oemler, A. Jr., Butcher, H., Sharples, R.M., 1997, *ApJS*, 110, 213 (S97)

Steidel, C.C., Adelberger, K.L., Giavalisco, M., Dickinson, M.E., Pettini, M., 1999, *ApJ*, in press

Trager, S.C., Faber, S.M., Dressler, A., Oemler, A. Jr., 1997, *ApJ*, 485, 92

Treu, T., et al., 1999, *A&A*, submitted (astro-ph/9808282).

Yan, L., McCarthy, P.J., Freudling, W., Teplitz, H.I., Malumuth, E.M., Weymann, R.J., Malkan, M.A., 1999, *ApJL*, in press.

Fig. 1. The VLA 1.4-GHz map overlayed as a contour plot on the *HST NICMOS* F160W mosaic. The radio sources are identified in large font using the numbering scheme of Smail et al. (1997). The galaxies labelled with the smaller font represent other spectroscopically identified galaxies (with the exception of #333) from the catalog of Dressler et al. (1999), these are similarly numbered using the S97 identifications. The dashed line shows the overlap on this field of the *WFPC2* F702W exposure from S97. The radio contours are at 12, 25, 50, 100 and 200 μ Jy per beam. North is top and east is left in this figure.

Fig. 3. The groups of *NICMOS* F160W, F702W–F160W and *WFPC2* F702W images for each of the ten galaxies selected from the VLA 1.4-GHz map of Cl 0939+4713. The F160W and F702W images provide restframe *J*- and *B*-band views of the galaxies and these are shown with a linear intensity scale, while the color image is constructed from the difference of the log-scaled F160W and F702W images. In the F702W–F160W color image lighter regions represent redder areas of the galaxy, the typical color range is roughly $R_{702} - H_{160} = 2.4\text{--}3.2$ (black to white). The panels are labelled with the catalog number, morphological type, spectral type and disturbance index (from S97 and D99). Each panel is $10'' \times 10''$ (equivalent to 65 kpc square at the cluster redshift) with north top and east left and the panels are ordered on morphology. Note that #640 lies in the extreme corner of the *WFPC2* field and #230 falls on a chip-boundary in the F702W exposure. All of the galaxies are confirmed cluster members with the exception of #640 which is a foreground field galaxy and #230 which has no spectroscopic identification.

Fig. 4. A comparison sample of spectroscopically-confirmed cluster galaxies which show no detectable radio emission in the VLA map above a 1.4-GHz flux of $S_{1.4} = 27\mu$ Jy. This figure includes all the spectrally-active members of this sample and again is ordered on morphology. The panels are labelled with the galaxy ID, morphology and disturbance index, *D*, from S97 and the spectral classification from D99.

This figure "f1.gif" is available in "gif" format from:

<http://arxiv.org/ps/astro-ph/9905354v1>

This figure "f3.gif" is available in "gif" format from:

<http://arxiv.org/ps/astro-ph/9905354v1>

This figure "f4.gif" is available in "gif" format from:

<http://arxiv.org/ps/astro-ph/9905354v1>